
Article:
Gyftakis, K.N. orcid.org/0000-0002-9730-4267, Salinas, M. orcid.org/0009-0002-2131-6699, Trachalakis, N. et al. (2 more authors) (2025) Zero-sequence flux analysis aiming for reliable detection of broken rotor bars in induction motors. IEEE Transactions on Industry Applications. ISSN 0093-9994

https://doi.org/10.1109/tia.2025.3574044

Zero-Sequence Flux Analysis Aiming for Reliable Detection of Broken Rotor Bars in Induction Motors

Konstantinos N. Gyftakis, *Senior Member, IEEE*, Marios Salinas, Nikolaos Trachalakis, Zihao Song and Panagiotis A. Panagiotou, *Member, IEEE*

Abstract— **Rotor electrical faults may appear in induction motors. Typically, this fault evolves at a slow rate, thus making it prominent for early detection. However, it has been shown that multiple breakages at non-adjacent positions may not create signatures when the MCSA is applied. Although the analysis of the stator current during the start-up transient can reveal this fault reliably, there are several industrial applications where the motors do not experience frequent start-ups making such methods obsolete. This paper addresses this need, that of detecting the fault reliably at steady state. The authors have utilised the zero-sequence stray flux and show that this methodology can identify the fault independently from the stator winding connection to the supply or the size and geometry of the motor.**

Index Terms—**broken bars, condition monitoring, fault diagnosis, finite element analysis, induction motors**

I. INTRODUCTION

THE reliability of induction motors is critical in industrial applications. This is to ensure continuous productivity, while any interrupted process will lead to high financial losses [1]. This is the motivation behind the tremendous interest of the community in the development of successful condition monitoring strategies.

Rotor electrical faults usually manifest themselves as broken/cracked rotor bars/end rings in cage induction machines. This fault type is not immediately catastrophic, although rare cases have been reported where rotor faults damaged the stator windings leading to a motor breakdown [2]-[3]. Moreover, it has been shown that when a bar breaks, the adjacent bars are overcharged with higher current densities and are expected to break next [4]. Despite that, cases have been reported where non-adjacent bars were found broken [5]. This phenomenon is mostly associated with rotor cages fabricated from copper, notably larger machines. It is important to note that the cost of a failure may be very high, mainly due to the interruption of the production process [6].

Non-adjacent broken bars may lead to false negative diagnostic alarms when the Motor Current Signature Analysis (MCSA) is employed [7]. This has been shown to happen when two breakages exist at half pole pitch apart [8]. In this case, the magnetic asymmetry of the first broken bar is neutralised by the second, leading to absence of fault-related signatures or signatures of weak amplitudes that do not cause alarm.

Several methods have been developed for detecting broken rotor bars in induction motors. Among them, the MCSA [9], the stray flux monitoring [10] and the torque [11] have all been applied with success. Late findings have demonstrated the advantages of the use of the triplet harmonics diagnostics in delta-connected induction motors [12]. In terms of signal processing, when the motors are analysed during transient operation such as the start-up, different methods can be found in the literature [13]. Among those, the STFT [14], Wavelets [15], MUSIC [16], Dragon Transform [17] and others are the most prominent. Recent work has shown promising diagnostic results in closed-loop control operation [18].

The transient analysis has shown satisfying results when non-adjacent broken bars are to be detected [19]. This is due to the combination of skin effect and high rotor current that magnify the magnetic asymmetry due to the fault, thus offering a distinguishable harmonic trajectory over time. However, there are many industrial applications where induction motors are not subject to frequent start-ups. This is due to the fact that the lifetime of the motor is dependent on the number of starts [20]. Instead, they operate continuously for long periods. In those cases, transient analysis-based methods are rather redundant. As such, there is a need for the development of reliable methods, capable for detection of broken bars, independently from their location, while the motors are at steady state. The frequency extraction is a recent method that has worked successfully in such cases [21]. The only drawback of this method is the high computational cost, since it relies on a two-stage signal processing approach.

In this paper, the authors are proposing the zero-sequence flux for the monitoring of non-adjacent broken bars in induction motors at steady state [22]. The work has been carried out with extensive finite element analysis and experimental testing, while motors of different power and voltage levels have been examined. The zero-sequence current analysis method has been proposed in the past for broken bar detection and proved to be successful. However, this method has practical limitations. It cannot be applied in Y-connected motors and for Δ-connected ones, it requires access to the phase currents. In other relevant papers the zero-sequence signal is acquired by means of signal

Konstantinos N. Gyftakis, Marios Salinas and Nikolaos Trachalakis are with the School of Electrical and Computer Engineering, Technical University of Crete, Akrotiri Campus, Chania, 73100, Greece (e-mail: k.n.gyftakis@ieee.org).

Zihao Song and Panagiotis A. Panagiotou are with the Department of Electronic and Electrical Engineering, The University of Sheffield, Sheffield S1 4DE, UK (e-mail: p.panagiotou@sheffield.ac.uk).

injection in the motor [23]-[24]. It will be shown in this work that the zero-sequence flux method resembles the advantages of the zero-sequence current without any limitations, as it can be applied on any induction motor because it does not depend on the stator winding. Moreover, the flux monitoring overcomes disadvantages of signature monitoring in the machine current, the spectrum of which is dependent on the distribution of the stator winding, a fact to have been related to several cases of false positive/negative diagnostic alarms [25]-[26].

II. FEA Models

To explore the impact of the motor size, geometry and stator winding configuration, two different induction motors have been simulated with Finite Element Analysis (FEA) using the commercially available software package Simcenter Magnet provided and supported by Infologic Design Ltd UK. The respective nominal characteristics of each motor are shown in Table I. The smaller motor has an aluminium cage, while the other has a copper one. Their numbers of poles are different, as are their rotor slot numbers and slots per pole numbers. Finally, the two motors and their respective magnetic flux distributions are shown in Fig. 1 (healthy nominal operation).

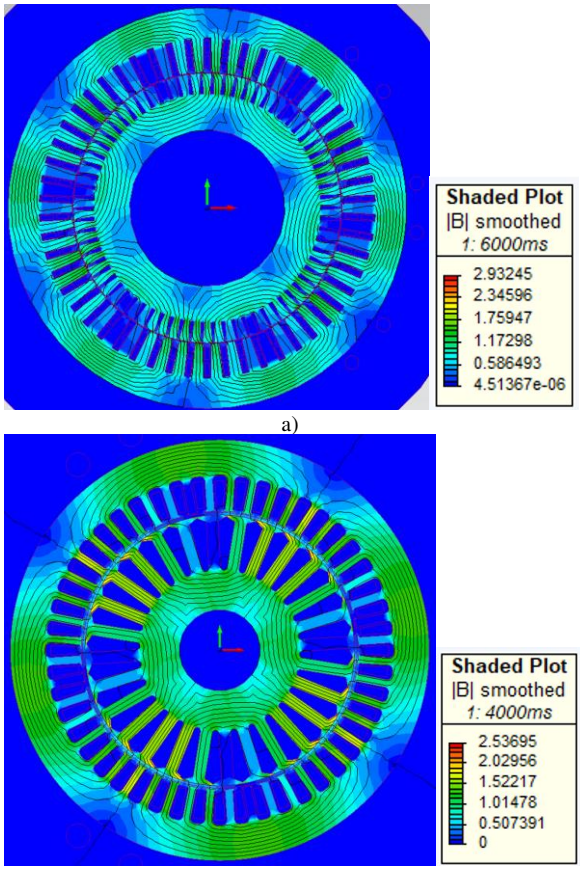

Fig. 1. Spatial distribution of the magnetic flux for: a) Motor A and b) Motor B, while at steady state under healthy condition.

III. Analysis of the Stator Current

Firstly, the stator current is analysed for all the studied cases. The analysis concerns both the steady state and the starting transient.

A. Steady State Analysis

The respective MCSA results are presented in Fig. 2 for both motors. The main broken bar fault signatures at $f_s - 2sf_s$ are marked with arrows (Fig. 2) and their amplitudes are shown in Table II, alongside with the exact frequency at which they appear. The right sideband is well known to depend on the inertia of the electromechanical system, so it is not studied here in detail (although it shows the same behaviour with the left sideband). It is not possible to have two broken bars at exactly half pole pitch, in neither of the motors. However, the closest to that distance is selected. In the case of Motor A, two possible positions are studied (1st and 5th or 6th broken bars). The results demonstrate how the fault may be masked leading to weak fault signatures that have amplitudes even less than those of 1 broken bar. Considering the empirically established threshold of -42 dB, it is evident that both motors would pass as healthy although two non-adjacent broken bars exist.

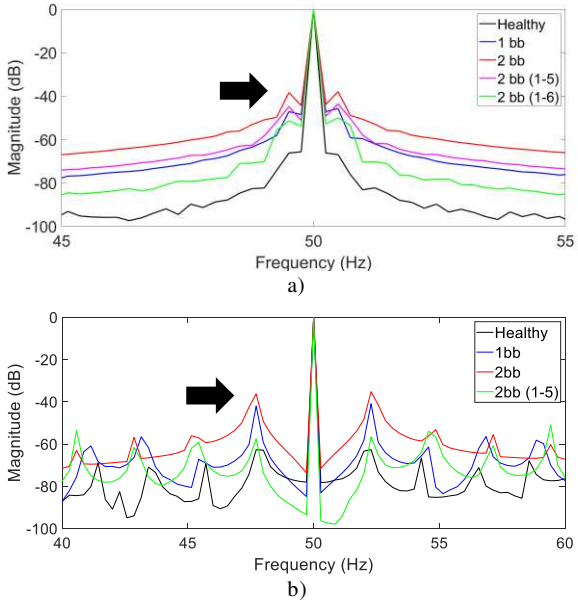

Fig. 2. MCSA of: a) Motor A and b) Motor B under healthy and faulty conditions at steady state under rated load (FEA result).

TABLE I
MOTORS' RATED PARAMETERS

Parameter	Motor A	Motor B
Voltage	6.6 kV	690 V
Power	1.14 MW	4 kW
Current	117.4 A	6.5 A
Pole pairs	3	2
Stator slots	54	48
Rotor slots	70	28
Stator connection	Y	Y

TABLE II
MCSA – LEFT SIDEBAND AMPLITUDES

Motor condition	Motor A	Slip (%)	Motor B	Slip (%)
Healthy	-66.24 dB	0.37	-62.85 dB	2.16
1 broken bar	-47.16 dB	0.38	-41.96 dB	2.25
2 broken bars (1-2)	-38.35 dB	0.39	-36.27 dB	2.37
2 broken bars (1-5)	-44.82 dB	0.387	-57.53 dB	2.35
2 broken bars (1-6)	-51.39 dB	0.386		

B. *Transient Analysis*

Motor A is set to accelerate from stall. The motor does not carry any mechanical load on its shaft. The Short Time Fourier Transform (STFT) has been applied to the stator currents and the results are presented in Fig. 3 for all the cases studied. For the generation of the motor's spectrogram, a window length of 2048 samples was needed for the accurate usage of the Kaiser filter with the beta parameter locked at 7.95. The signal length is 14500 samples, and the sample frequency is 5 kHz. When the motor is healthy, the main harmonics noticed in the spectrogram are the fundamental and the 5th.

However, when a broken bar fault happens, more harmonic trajectories are observed. Specifically, the well- known V-shape below the fundamental is noticeable $(1-2sf_s)$. Other trajectories such as the $1+2sf_s$, $5-4sf_s$ and the sidebands of the Rotor Slot Harmonics (RSH) are also easily observed. All the trajectories are enhanced in terms of amplitude when two adjacent broken bars exist in the motor. On the other hand, the trajectories are visible in one of the two non-adjacent broken bars cases (1st and 5th), however their amplitudes are not strong. Ths is worse for the motor with non-adjacent broken bars 1 and 6. The trajectories are the same, however the amplitudes of the harmonics are significantly lower. Considering that in a real motor, the fault related signatures exist due to inherent manufacturing asymmetries even in healthy machines, the danger of misdiagnosis is present even under transient analysis.

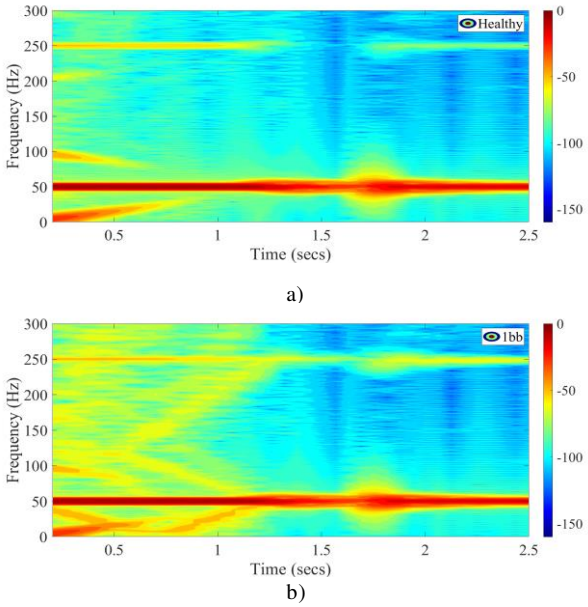

a)

b)

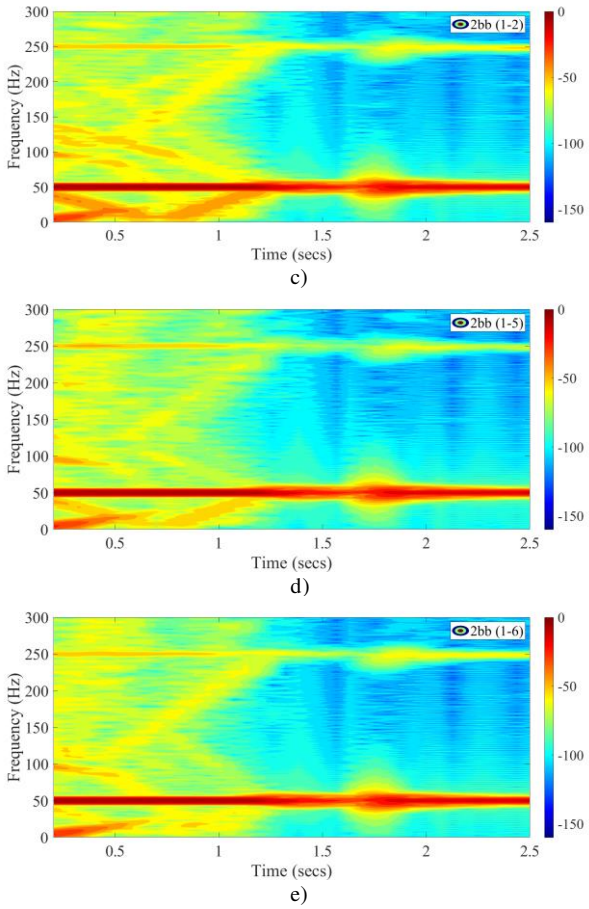

c)

d)

e)

Fig. 3. STFT current spectrograms of Motor A under: a) healthy condition, b) 1 broken bar, c) 2 adjacent broken bars, d) 2 non-adjacent broken bars (1-5) and e) 2 non-adjacent broken bars (1-6) during the start-up transient (FEA result).

IV. ZERO-SEQUENCE FLUX MONITORING

A. *Harmonic Index of the Stray Flux Monitoring*

The stray flux monitoring has a similar harmonic index with the line current, meaning that all the harmonics of the line current will be present in the stray flux. Under healthy operation, the stray flux will contain the odd multiples of the supply frequency minus the triplets $(6k\pm1)f_s$. Broken bar fault signatures are expected at frequencies [7]:

$$f_{bb}=\left[\frac{k}{p}(1-s)\pm s\right]f_s. \quad (1)$$

One main difference between the harmonic index of the stray flux and the stator current is the existence of the odd triplets in the former, as well as the homopolar RSH. Those harmonics are cancelled in the stator current due to the formation of the winding to create the magnetic poles in space.

Moreover, it has been shown that rotor electrical faults give rise to harmonics at $f_s\pm k\frac{(1-s)}{p}f_s$ [27]. Typically, these harmonics are associated with mixed eccentricity faults when the MCSA is applied, however electromagnetic rotor faults will affect this signature in the stray flux spectra, as well as eccentricity.

Prior works [28] have proven the superiority of the zero-sequence current (ZSC) analysis over the MCSA. When it comes to the broken bar fault detection, the fundamental of the

ZSC exists at $3f_s$. Searching for sidebands around the fundamental ZSC harmonic has three distinct advantages:

- The fault generates two main harmonics in the ZSC ($3f_s - 2sf_s$ *and* $3f_s - 4sf_s$) instead of one in the MCSA ($f_s - 2sf_s$).
- The higher the frequency, the higher the amplitude of the signatures due to Faraday's law of induction.
- The higher the frequency, the stronger the skin effect in the rotor and thus stronger the magnetic asymmetry close to the airgap, leading again to stronger fault signatures.

Another advantage of the ZSC is its ability to detect other faulty conditions as well, some of which are not easily detected by the MCSA, and this is due to the cancellation of the stator MMF harmonics in its spectrum when the machine is healthy and perfectly symmetrical. This is a common quality element between the ZSC and the ZSF.

Moreover, it is now known that the flux signal has multiple advantages over the stator current one. Its independence from the motor geometry and stator winding poles topology and poles, permits the detection of many faulty conditions in the flux that may go unnoticed with MCSA [7]. Therefore, the ZSF signal which is calculated by the flux signals of a richer harmonic index than the stator currents, is expected to offer a better diagnostic capability. Despite the above, the main critical advantage of the ZSF over the ZSC is that the ZSC cannot be applied in motors that are Y connected (no neutral). The ZSF carries all the advantages of the ZSC, and it can be applied on any motor independently from the stator winding configuration. Additionally, it is critical to mention that new empirical thresholds should be adopted since the tracking of harmonics at higher frequencies will boost their amplitudes well above the MCSA threshold of -42 dB.

In this work, the ZSF is calculated from the signals obtained by three radial stray flux sensors with 1000 turns and a diameter of 110 mm each, located at 120 electrical degrees apart. The ZSF is expected to have the same advantages, plus the ability to offer additional signatures compared to the ZSC. The spectra between 50 Hz and 190 Hz are shown for both motors in Fig. 4. Moreover, the frequency area of the ZSF fundamental is shown in Fig. 5. The amplitudes of the fault related signatures, around the fundamental, are presented in Table III. From these results, the following key conclusions can be drawn:

- The absolute amplitude of the fault signatures is significantly higher than those of the current. This is a predicted outcome due to reasons explained earlier in this paper.
- The amplitude increase of the signatures is higher compared to those in the corresponding stator current spectrum.
- Both signatures next to the fundamental are very clear in all the examined faulty cases. However, the $3f_s - 4sf_s$ has better fault severity sensitivity. On the other hand, the signature located at $3f_s - 2sf_s$ may offer amplitudes weaker than those of a single-bar fault (1 broken bar). Still, they are easily distinguishable, but this harmonic does not render a monotonic trend with respect to the fault severity.

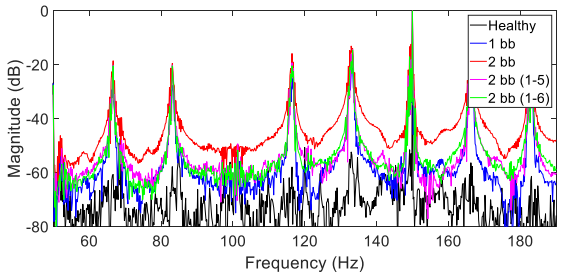

a)

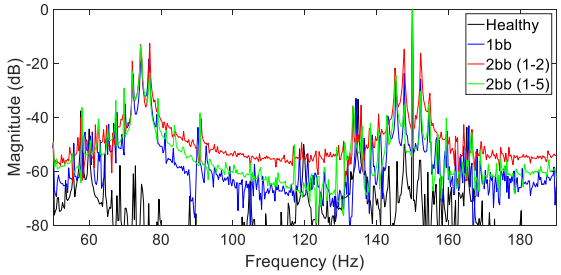

b)

Fig. 4. ZSF spectra of: a) Motor A and b) Motor B while at steady state under rated load (FEA result).

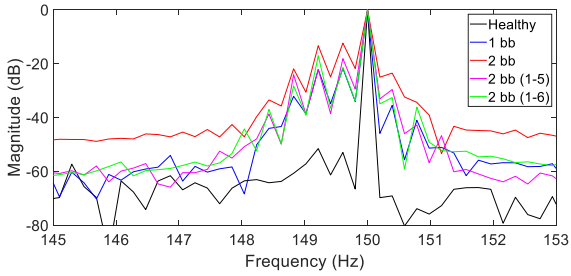

a)

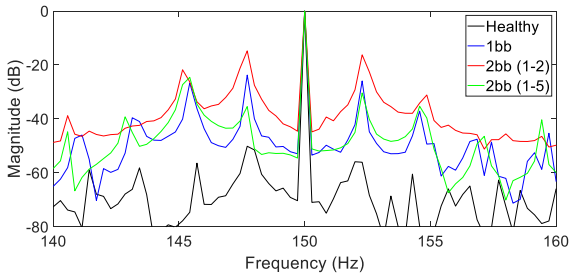

b)

Fig. 5. ZSF results for: a) Motor A and b) Motor B while at steady state under rated load (FEA result).

TABLE III

ZSF – LEFT SIDEBAND AMPLITUDES

	Motor A		**Motor B**	
Motor condition	$3f_s - 2sf_s$	$3f_s - 4sf_s$	$3f_s - 2sf_s$	$3f_s - 4sf_s$
Healthy	-52.94 dB	-51.52 dB	-50.13 dB	-56.40 dB
1 broken bar	-21.74 dB	-22.09 dB	-23.74 dB	-26.26 dB
2 broken bars (1-2)	-12.36 dB	-13.30 dB	-14.77 dB	-21.78 dB
2 broken bars (1-5)	-18.11 dB	-22.09 dB	-35.42 dB	-24.56 dB
2 broken bars (1-6)	-21.41 dB	-17.03 dB		

Moreover, the $f_s \pm k\frac{(1-s)}{p}f_s$ are shown to increase by more than 40 dB in both motors when there is a fault present, and independently from the condition. Those harmonics are also escorted by additional fault related sidebands distanced by $2ksf_s$.

V. Load Impact

The applied load is known to affect the reliability of the broken bar fault detection. Specifically, the load reduction leads to weaker rotor current, while the slip frequency is reduced as well. This shifts the signatures of the current closer to the fundamental leading to potential misdiagnosis and false negative alarms. This is dependent on the size of the motor. Large motors operate at speeds very close to the synchronous one and therefore the broken bars are impossible to detect at no-load operation. As shown in Fig. 6-a, MCSA is completely incapable of detecting the broken rotor bar fault, of any severity, if Motor A is loaded by half the rated load (5.5 kNm), a condition very usual in real applications. On the other hand, Motor B still has a significant enough slip at half load (13 Nm) to permit reliable detection with both ZSF signatures. It is compelling that the $3f_s - 4sf_s$ signature has similar amplitudes for two broken bars, independently from their respective location on the rotor. The amplitudes of the respective fault signatures are shown in Table IV.

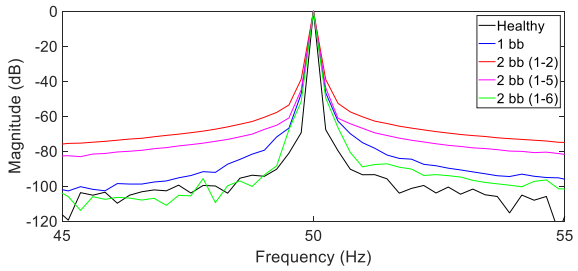

a)

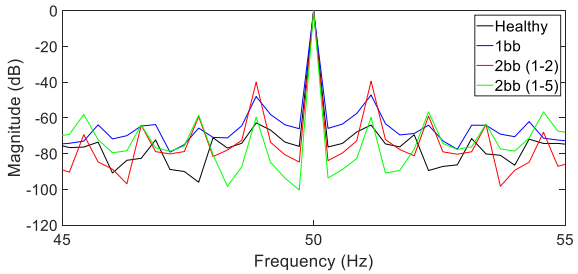

b)

Fig. 6. MCSA results for: a) Motor A and b) Motor B at steady state under half the rated load (FEA result).

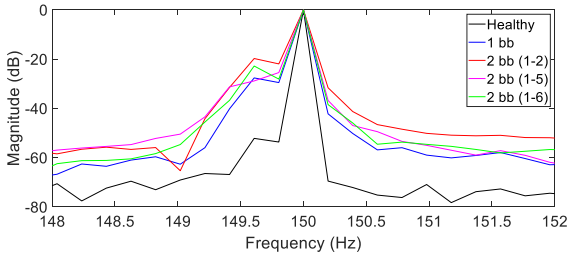

a)

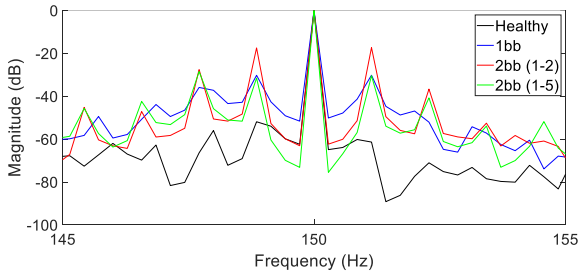

b)

Fig. 7. ZSF results for: a) Motor A and b) Motor B at steady state under half the rated load (FEA result).

TABLE IV
$3f_s - 4sf_s$ AMPLITUDES OF ZSF

Motor condition	Motor A	Motor B
Healthy	-52.18 dB	-55.95 dB
1 broken bar	-27.63 dB	-35.87 dB
2 broken bars (1-2)	-19.75 dB	-27.55 dB
2 broken bars (1-5)	-28.85 dB	-28.46 dB
2 broken bars (1-6)	-22.79 dB	

VI. ZSF Analysis During Transients

Although the main scope of this work is to develop a method for steady state analysis, it is important that the same method has fault sensitivity during the starting transient of the motor. For this purpose, the ZSF is studied under transient conditions as well.

The expected trajectories of Motor A are shown on Fig. 8. This includes the production of broken bar fault sidebands around the mechanical frequency generated harmonics ($f_s \pm k\frac{(1-s)}{p}f_s \pm 2ksf_s$), as well as the stator-related MMF ones at the frequency of $(\left[\frac{k}{p}(1-s) \pm s\right]f_s)$. Moreover, the spectrograms of the studied cases are presented in Fig. 9. The simulation results agree with the expected trajectories.

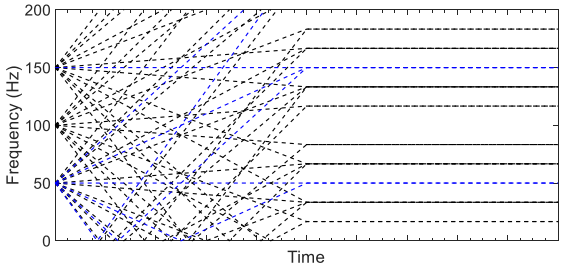

Fig. 8. Expected broken bar fault harmonic trajectories in the ZSF of a 6-pole motor.

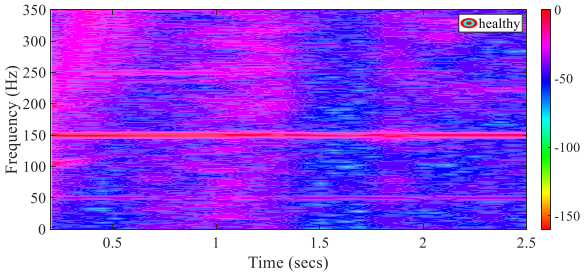

a)

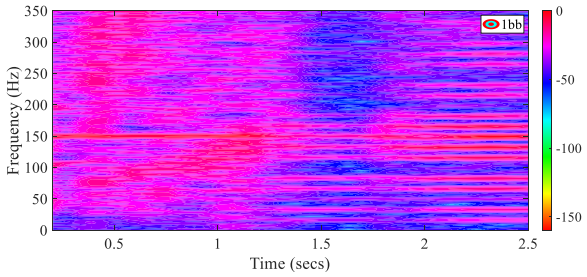

b)

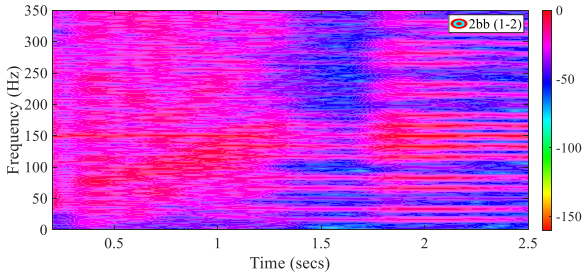

c)

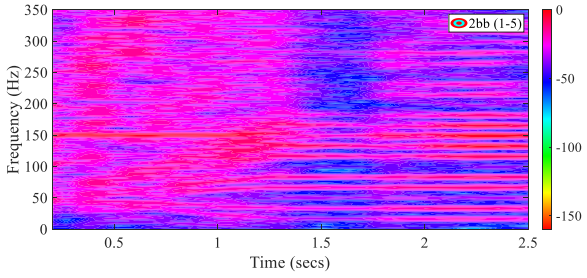

d)

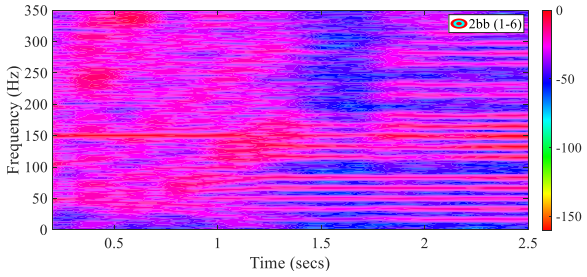

e)

Fig. 9. STFT spectrograms of the ZSF, of Motor A under: a) healthy condition, b) 1 broken bar, c) 2 adjacent broken bars, d) 2 non-adjacent broken bars (1-5) and e) 2 non-adjacent broken bars (1-6) during the start-up transient (FEA result).

VII. Experimental Testing

For the purposes of experimental validation, an electric machine dynamometer was utilised that incorporates an induction motor coupled with a permanent magnet synchronous machine (PMSM). This test rig used for the acquisition of the experimental data was developed to serve the purpose of an electric vehicle emulator system as described in [29]. The configuration of this system enables electric vehicle emulation features, where the machine under test is driven in different loading conditions by the load machine. The induction motor of this test bed is a 1.1 kW, 4-pole, 28 V induction motor at 50 Hz, with 36 stator slots, 46 rotor bars, and a Δ-connected distributed winding. The characteristics of the experimental motor are given in Table V, while Fig. 10-a illustrates the electric vehicle emulator system with the instrumentation used for the acquisition of measurements. Further, Fig. 10-b depicts the rotors drilled at different locations with the arrows indicating the location of the bar breakages on the rotor cage.

TABLE V
Characteristics of Tested Motors

Characteristics	Value
Supply frequency	50 Hz
Stator winding connection	Δ
Output power	1.1 kW
Rated voltage	28 V
Rated current	45.6 A
Number of pole pairs	2
Synchronous speed	1500 rpm
Number of stator slots	36
Number of rotor bars	46

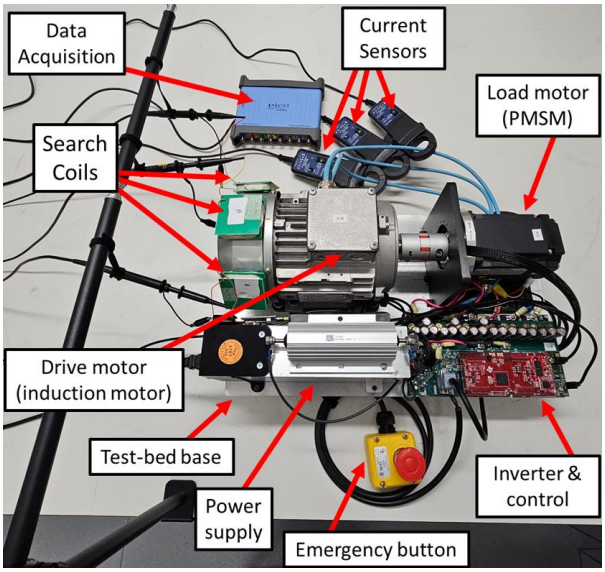

a)

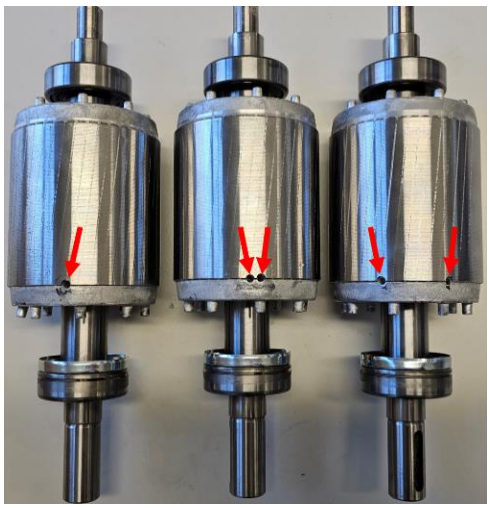

b)

Fig. 10. Hardware used for experimental measurements: a) electric vehicle emulator system and instrumentation for data acquisition, and b) rotors with broken bars at various locations: 1 broken bar (left), 2 adjacent broken bars (middle), 2 non-adjacent broken bars at half pole pitch distance (right).

Several identical rotors were drilled with precision machining at different locations of the rotor cage to emulate the bar breakage scenarios (arrows in Fig. 10-b). The cases examined correspond to the healthy motor and three different cases of rotor breakages, notably the single-bar fault, two adjacent broken bars, and two non-adjacent broken bars at half pole pitch. The experimental measurements were acquired with the machine operating at different loading conditions in open-loop control mode, consistently replicating the simulations setting presented in this work, as well as at other load levels for further validation beyond the FEA cases. The experimental data were acquired with a sampling frequency of 20 kHz.

The stator current signals of each motor were measured via three current sensors with sensitivity of 10 mV/A and an accuracy of $\pm 1\%$ of reading at $\pm 100/\pm 500$ mA. The stray flux was captured outside of the yoke of the machine with the use of three identical flux sensors that were designed in-house and built manually in the laboratory. These search coils consist of 1500 turns that were formed on a 40x40 mm^2 coil reel and covered on both reel ends by 55x55 mm^2 salient square edges. The whole 8mm slot height was fully covered by the copper windings, with the conductors having a diameter of 0.1mm and an ohmic resistance of 3.4 Ω/m. The flux signals were harvested by voltage probes connected to one end of each search coil, while the other ends were grounded (search coils in Fig. 10-a). The three sensors were carefully placed symmetrically around the machine with a spatial phase difference corresponding to the angle of 120 electrical degrees.

The current and stray flux signals measured were logged onto an oscilloscope with eight channels, a 12-bit resolution, 20 MHz bandwidth and a serial bus decoding with 256 MS buffer memory. Each of the six signal waveforms (three current and three stray flux signals) were connected to a separate channel and the signals were captured in 4 frames of 50s duration with a sampling rate of 20 kHz. This ensures that the motor's steady state is greatly covered, and reliable results can be drawn.

A. Motor Current Signature Analysis

The results of MCSA are shown in Fig. 11 for all the studied cases. The motor operates under load at approximately 1388 rpm (healthy) with small variations under fault, that enable good visibility of the different spectra and signatures. The amplitude of the left characteristic broken bar fault sideband is tracked for all cases and marked with arrows. Moreover, its amplitude has been extracted and presented in Table VI. It is evident that MCSA is completely unreliable to detect non-adjacent broken rotor bars since this condition perfectly resembles the healthy motor. A signature is produced at the expected frequency; however its amplitude is the same as in the healthy motor (Table VI) and lower than the established empirical threshold of -42 dB. Even newly manufactured motors may have inherently this signature due to a small level of cage porosity and magnetic anisotropy of the rotor iron core, both conditions that originate from the manufacturing of the motor. Therefore, the motor with non-adjacent broken rotor bars would pass as a healthy motor if only the MCSA was applied. However, for the other faulty cases, the produced signatures exceed the empirical threshold of -42 dB, clearly revealing a broken rotor bar fault. The results agree with those from FEA in Fig. 2.

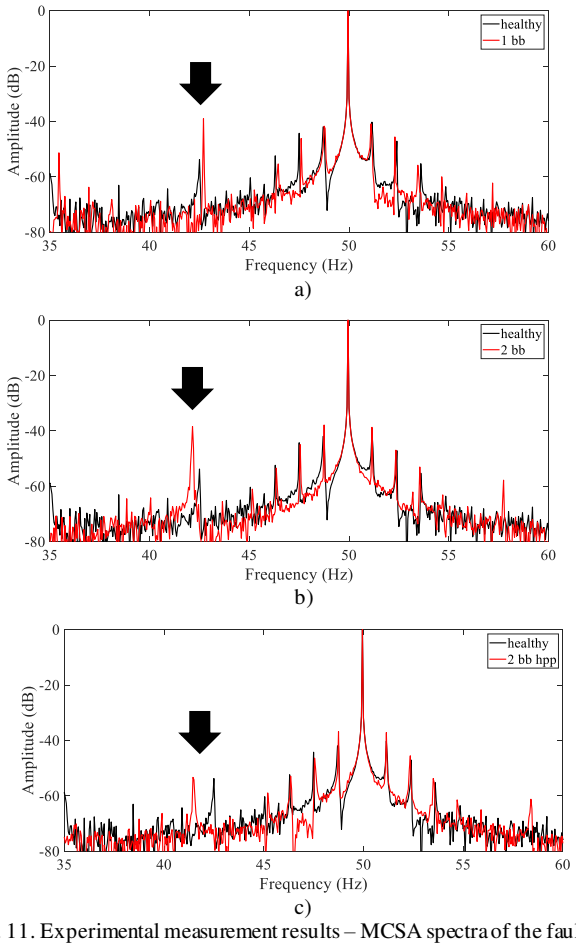

Fig. 11. Experimental measurement results – MCSA spectra of the faulty cases (red): a) motor with a broken bar, b) motor with two adjacent broken bars and c) motor with two non-adjacent broken bars versus the healthy case (black).

TABLE VI
MCSA – LEFT SIDEBAND AMPLITUDES

Motor condition	Amplitude	Amplitude Difference	Slip (%)
Healthy	-53.74 dB		7.5
1 broken bar	-38.99 dB	14.75 dB	7.3
2 adjacent broken bars	-38.39 dB	15.35 dB	7.85
2 non-adjacent broken bars	-53.32 dB	0.42 dB	8.5

B. Stray Flux Analysis

It is well known that one significant difference between the stator current and stray flux spectra is the presence of strong harmonics related to mechanical speed, $f_s \pm (1-s)\,{}^{f_s}/_{p}$ when a broken bar appears [25]. This is a major difference between the two, while the classical broken bar fault sidebands around

the fundamental are expected in both cases in the same manner. Fig. 12 depicts the frequency area 24-30 Hz. It is easy to notice the mechanical frequency related signature in all the cases (marked with arrow). It even exists in the healthy motor due to inherent asymmetries such as the cage porosity, magnetic anisotropy and mixed eccentricity. However, for the cases of 1 and two adjacent broken bars, one can easily notice the production of additional broken bar fault signatures at $f_s \pm (1-s)^{f_s}/_{p} \pm 2sf_s$, that have been marked with red arrows. On the other hand, when two non-adjacent bars break those signatures are almost absent at the noise floor level (Fig. 12-c).

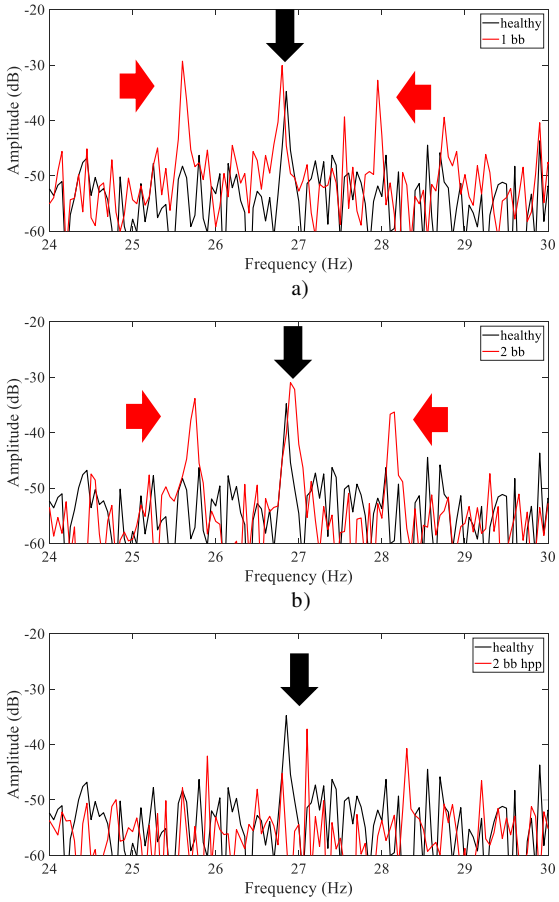

Fig. 13. Experimental measurement results – Stray flux spectrum of the faulty cases (red) versus the healthy case (black).

C. Zero-Sequence Flux Analysis

The three sensors have been placed on the stator by 120 degrees electrical phase difference. The three sensor signals are shown Fig. 14-a. Then, the signals are added over time leading to the zero-sequence flux signal which is shown at steady state in Fig. 14-b.

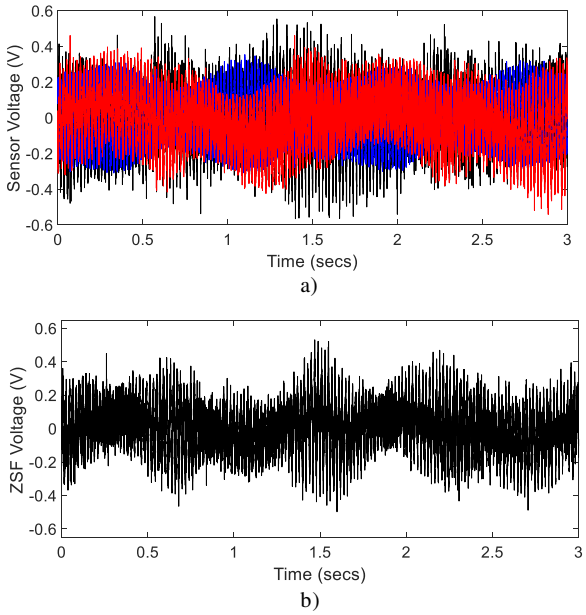

Fig. 14. Experimental measurement results: a) The stray flux signals and b) the zero sequence flux signal of the healthy motor at steady state.

The ZSF spectra around the fundamental 150 Hz harmonic for both healthy and faulty conditions are presented in Fig. 15, with the sideband amplitudes summarised in Table VII. The sidebands are all characterised by a distinctive amplitude increase, despite the inherent cage manufacturing tolerances when one or two adjacent broken bars exist in the motor. For the case of the motor with two non-adjacent broken bars the signature at $3f_s - 2sf_s$ remains unaffected by the fault and is characterised by approximately the same amplitude with the healthy motor. However, the $3f_s - 4sf_s$ harmonic presents a great amplitude increase that can clearly reveal the fault reliably. This outcome verifies with accuracy the FEA results shown earlier in Table III for motor B, which is in a similar power range with the tested motor.

Furthermore, the motor behaviour has been studied during the start-up transient for all cases. The spectrograms are shown in Fig. 16. It is obvious that the harmonic $3f_s - 4sf_s$ creates a unique trajectory in all the faulty cases (marked with arrows), however it is absent in the healthy motor. This harmonic's trajectory begins at 50 Hz, then drops at 0 Hz for slip 0.75 and finally increases up to the steady state frequency that depends on the steady state slip right before the 3rd harmonic. The experimental results prove that the zero-sequence flux signal is advantageous over the other two methods since it reveals the fault reliably at steady state and during transient conditions.

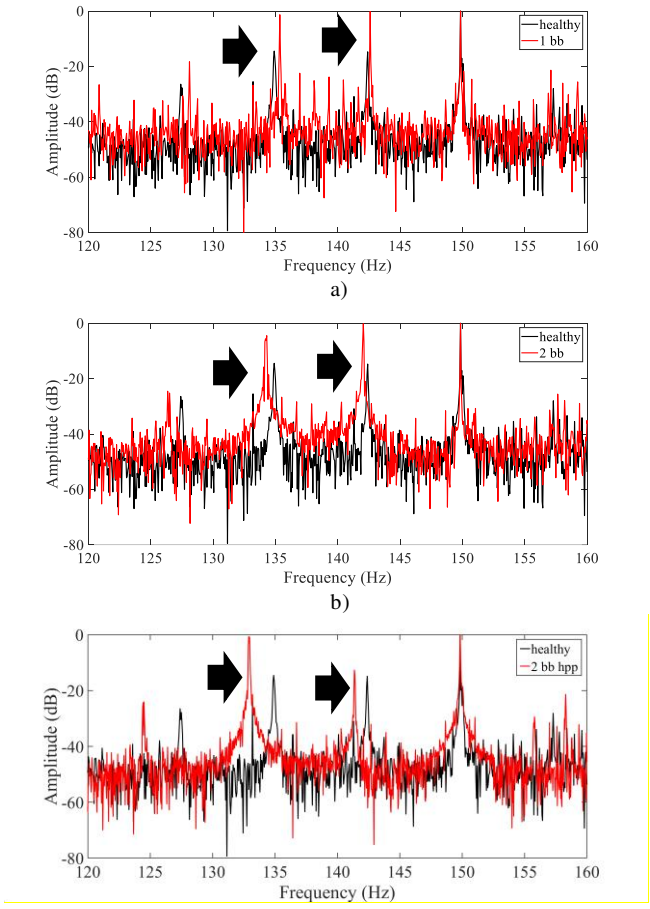

Fig. 15. Experimental measurement results – ZSF spectra of the healthy motor (black) over the faulty ones (red) where: a) 1 broken bar, b) 2 adjacent broken bars and c) 2 non-adjacent broken bars while the motor is at steady state.

TABLE VII
LEFT SIDEBAND AMPLITUDES OF ZSF

Motor condition	$3f_s - 2sf_s$	Amplitude difference	$3f_s - 4sf_s$	Amplitude difference
Healthy	-14.73 dB		-14.46 dB	
1 broken bar	-0.19 dB	14.54 dB	-1.33 dB	13.13 dB
2 adjacent broken bars	-0.18 dB	14.55 dB	-4.48 dB	9.98 dB
2 non-adjacent broken bars	-12.63 dB	2.1 dB	-0.61 dB	13.85 dB

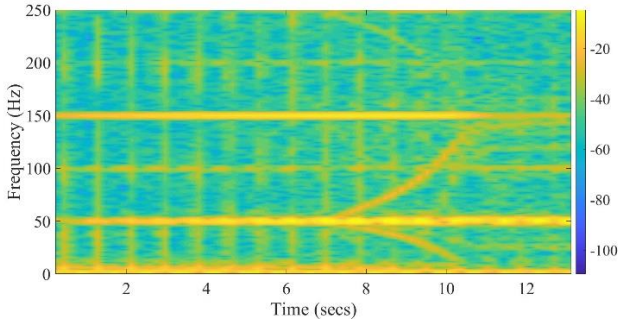

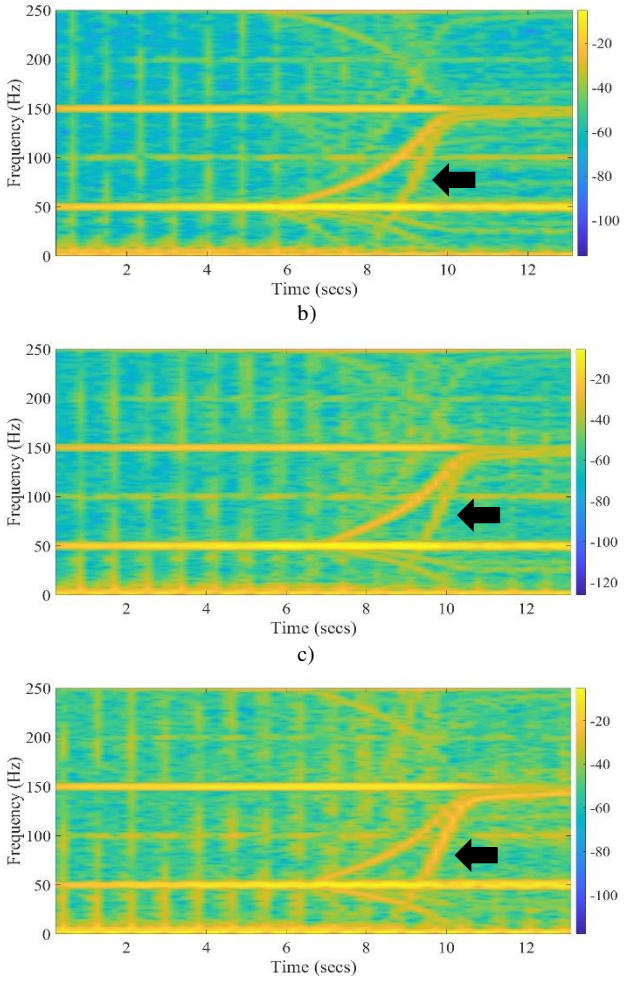

Fig. 16. Experimental measurement results – ZSF spectrogram during the start-up transient of a) the healthy, b) the motor with one broken bar, c) the motor with two adjacent broken bars and d) the motor with two non-adjacent broken bars.

VIII. CONCLUSIONS

In this work, the authors propose the use of the Zero-Sequence Flux (ZSF) analysis as a reliable diagnostic approach to detect rotor electrical faults in induction motors and avoid false negative diagnostic alarms due to non-adjacent broken rotor bars. The authors have demonstrated the advantages of the method over the stator current and stray flux analysis at steady state as well as during transient conditions with extensive FEA simulations and experimental testing. The evident plethora of fault-generated harmonics in the ZSF spectra makes this signal ideal for fault detection. Additionally, the paper proves experimentally for the first time that the ZSF signal analysis is advantageous compared to both MCSA and flux monitoring at steady state for non-adjacent broken rotor bar cases. The experimental results match those of the simulations and depict the $3f_s - 4sf_s$ as a reliable indicator of the fault at both steady state analysis as well as under transient operation.

ACKNOWLEDGEMENTS

The authors would like to gratefully acknowledge Thomas J. Templeman, Senior Technician of the Electrical Machines and Drives research group of the School of Electrical & Electronic Engineering at the University of Sheffield, for the valuable technical and workshop support during the acquisition of experimental measurements.

REFERENCES

[1] P. Zhang, Y. Du, T. G. Habetler and B. Lu, "A Survey of Condition Monitoring and Protection Methods for Medium-Voltage Induction Motors," *IEEE Trans. Ind. Appl.*, vol. 47, no. 1, pp. 34-46, Jan.-Feb. 2011.

[2] S. B. Lee et al., "Identification of False Rotor Fault Indications Produced by Online MCSA for Medium-Voltage Induction Machines," *IEEE Trans. Industry Appl.*, vol. 52, no. 1, pp. 729-739, Jan.-Feb. 2016.

[3] C. Yang et al., "Starting current analysis for condition monitoring of medium voltage induction motors in the steel industry," 2017 IEEE Industry Applications Society Annual Meeting, Cincinnati, OH, USA, pp. 1-9, 2017.

[4] G. Madescu, M. Biriescu, L. -N. Tutelea, M. Mot and I. Boldea, "Fast computation of bar over-currents in the faulty cage of induction motors with experimental validation," 2017 International Conference on Optimization of Electrical and Electronic Equipment (OPTIM) & 2017 Intl Aegean Conference on Electrical Machines and Power Electronics (ACEMP), Brasov, Romania, 2017.

[5] Y. Park, H. Choi, S. B. Lee and K. N. Gyftakis, "Search Coil-Based Detection of Nonadjacent Rotor Bar Damage in Squirrel Cage Induction Motors", *IEEE Trans. Ind. Appl.*, Vol. 56, No. 5, pp. 4748-4757, 2020.

[6] S. B. Lee, S. Park, S. Kim and S. Shim, "The Commercialization of Medium-Voltage Induction Motor Rotor Diagnostics Equipment: Helping Prevent In-Service Failures of Induction Motors and Processes," *IEEE Ind. Electr. Mag.*, vol. 16, no. 4, pp. 40-43, Dec. 2022.

[7] S. B. Lee et al., "Condition monitoring of industrial electric machines: State of the art and future challenges", *IEEE Ind. Elec. Mag.*, Vol. 14, No. 4, pp. 158-167, 2020.

[8] M. Riera-Guasp et al, "Influence of nonconsecutive bar breakages in motor current signature analysis for the diagnosis of rotor faults in induction motors," *IEEE Trans. Ener.* Conv. 25, no. 1, pp. 80–89, Mar. 2010.

[9] G. Niu, X. Dong and Y. Chen, "Motor Fault Diagnostics Based on Current Signatures: A Review," *IEEE Trans. Instr.. Meas.*, vol. 72, pp. 1-19, 2023.

[10] M. E. Iglesias-Martínez, P. Fernández de Córdoba, J. A. Antonino-Daviu and J. A. Conejero, "Detection of Nonadjacent Rotor Faults in Induction Motors via Spectral Subtraction and Autocorrelation of Stray Flux Signals," *IEEE Trans. Ind. Appl.*, vol. 55, no. 5, pp. 4585-4594, Sept.-Oct. 2019.

[11] D. V. Spyropoulos, P. A. Panagiotou, I. Arvanitakis, E. D. Mitronikas, and K. N. Gyftakis, "Extraction of Frequency Information for the Reliable Screening of Rotor Electrical Faults via Torque Monitoring in Induction Motors", *IEEE Trans. Ind. Appl.*, Vol. 57, No. 6, pp. 5949-5958, 2021.

[12] R. P. P. de Souza, D. Morinigo-Sotelo, V. Fernandez-Cavero, Ó. Duque-Perez, C. M. Agulhari and A. Goedtel, "The Analysis of Odd Triple Harmonics to Detect Broken Rotor Bar in Delta-Connected Induction Motors," *IEEE Trans. Ind. Appl.*, vol. 60, no. 6, pp. 8736-8744, Nov.-Dec. 2024.

[13] F. Filippetti, A. Bellini and G. -A. Capolino, "Condition monitoring and diagnosis of rotor faults in induction machines: State of art and future perspectives," 2013 IEEE Workshop on Electrical Machines Design, Control and Diagnosis (WEMDCD), Paris, France, pp. 196-209, 2013.

[14] J. A. Antonino-Daviu, I. Zamudio-Ramirez, R. A. Osornio-Rios and L. Dunai, "Fault Diagnosis in Electric Motors through the Analysis of Currents and Stray Fluxes," 2023 International Conference on Electromechanical and Energy Systems (SIELMEN), Craiova, Romania, pp. 1-7, 2023.

[15] G. R. Agah et al., "Broken Rotor Bar and Rotor Eccentricity Fault Detection in Induction Motors Using a Combination of Discrete Wavelet Transform and Teager–Kaiser Energy Operator," *IEEE Trans. Ener. Conv.*, vol. 37, no. 3, pp. 2199-2206, Sept. 2022.

[16] J. J. Yanez-Borjas, D. Camarena-Martinez, M. A. Vasquez-Barrera, R. J. Romero-Troncoso and D. Morinigo-Sotelo, "Experimental Validation of the Broken Rotor Bar Fault Evolution in Line-Fed Induction Motors," 2018 IEEE International Autumn Meeting on Power, Electronics and Computing (ROPEC), Ixtapa, Mexico, pp. 1-7, 2018.

[17] V. Fernandez-Cavero, J. Pons-Llinares, O. Duque-Perez and D. Morinigo-Sotelo, "Detection of Broken Rotor Bars in Nonlinear Startups of Inverter-Fed Induction Motors," *IEEE Trans. Ind. Appl.*, vol. 57, no. 3, pp. 2559-2568, May-June 2021.

[18] L. Mantione, T. Garcia-Calva, V. Fernandez-Cavero, L. Frosini and D. Moriñigo-Sotelo, "Broken Rotor Bar Detection in Closed Loop Inverter Fed Induction Motors Through Time-Frequency Techniques," *IEEE Trans. Ind. Appl.*, doi: 10.1109/TIA.2024.3482271, early access.

[19] J. Antonino-Daviu, H. Razik, A. Quijano-Lopez and V. Climente-Alarcon, "Detection of rotor faults via transient analysis of the external magnetic field," IECON 2017 - 43rd Annual Conference of the IEEE Industrial Electronics Society, Beijing, China, pp. 3815-3821, 2017.

[20] R. Curiac and S. Singhal, "Rotor and Stator Stresses During Starting of Induction Motors Used in Cement Industry Applications," 2009 IEEE Cement Industry Technical Conference Record, Palm Springs, CA, USA, pp. 1-11, 2009.

[21] P. A. Panagiotou, I. Arvanitakis, N. Lophitis , J. A. Antonino-Daviu and K. N. Gyftakis, "A New Approach for Broken Rotor Bar Detection in Induction Motors Using Frequency Extraction in Stray Flux Signals", *IEEE Trans. Ind. Appl.*, 2019, Vol. 55., No. 4, pp. 3501-3511, 2019.

[22] M. Salinas, N. Trachalakis, P. A. Panagiotou and K. N. Gyftakis, "Reliable Detection of Non-Adjacent Broken Rotor Bars via the Analysis of the Zero-Sequence Flux," 2024 International Conference on Electrical Machines (ICEM), Torino, Italy, pp. 1-6, 2024.

[23] P. M. de la Barrera, M. Otero, T. Schallschmidt, G. R. Bossio and R. Leidhold, "Active Broken Rotor Bar Diagnosis in Induction Motor Drives," in *IEEE Transactions on Industrial Electronics*, vol. 68, no. 8, pp. 7556-7566, Aug. 2021.

[24] M. Otero, P. M. de la Barrera, G. R. Bossio and R. Leidhold, "A strategy for broken bars diagnosis in induction motors drives," in *IEEE Latin America Transactions*, vol. 16, no. 2, pp. 322-328, Feb. 2018.

[25] S. B. Lee, J. Shin, Y. Park, H. Kim and J. Kim, "Reliable Flux based Detection of Rotor Cage Faults in Induction Motors," *13th IEEE International Symposium on Diagnostics for Electrical Machines, Power Electronics and Drives (SDEMPED)*, Dallas, TX, USA, pp. 160-166, 2021.

[26] Y. Park, M. Jeong, S. B. Lee, J. A. Antonino-Daviu and M. Teska, "Influence of Blade Pass Frequency Vibrations on MCSA-Based Rotor Fault Detection of Induction Motors," *IEEE Trans. Ind. Appl.*, vol. 53, no. 3, pp. 2049-2058, May-June 2017.

[27] K. N. Gyftakis, P. A. Panagiotou and S. B. Lee, "Generation of Mechanical Frequency Related Harmonics in the Stray Flux Spectra of Induction Motors Suffering from Rotor Electrical Faults", *IEEE Trans. Ind. Appl.*, 2020, Vol. 56, No. 5, pp. 4796-4803, 2020.

[28] K. N. Gyftakis and J. Kappatou, "The Zero-Sequence Current as a Generalized Diagnostic Mean in Δ-Connected Induction Motors," *IEEE Trans. Ener. Conv.*, Vol. 29, No. 1, pp. 138-148, Mar. 2014.

[29] T. Wray, P. A. Panagiotou, M. Masoud, H. O'Keeffe, R. Toqeer, A. Griffo, & P. Lazari. "A compact and modular remote access platform for enhanced practical education in power electronics, machines, and drives". In 13th International Conference on Power Electronics, Machines and Drives (PEMD 2024) (Vol. 2024, pp. 646-652). IET.). June 2024.

BIOGRAPHIES

Konstantinos N. Gyftakis (M'11-SM'20) received the Diploma in Electrical and Computer Engineering from the University of Patras, Patras, Greece in 2010. He pursued a Ph.D in the same institution in the area of electrical machines condition monitoring and fault diagnosis (2010-2014). Furthermore, he worked as a Post-Doctoral Research Assistant in the Dept. of Engineering Science, University of Oxford, UK (2014-2015). Then he worked as Lecturer (2015-2018) and Senior Lecturer (2018-2019) in the School of Computing, Electronics and Mathematics and as an Associate with the

Research Institute for Future Transport and Cities, Coventry University, UK. Finally, between 2019-2022, he worked as a Lecturer on Electrical Machines and a Member of the Institute for Energy Systems, University of Edinburgh, UK. He is currently a tenured Associate Professor with the School of Electrical and Computer Engineering, Technical University of Crete, Greece. His research interests focus in the fault diagnosis, condition monitoring and degradation of electrical machines. He has authored/co-authored more than 140 papers in international scientific journals and conferences Moreover, he is Secretary and International Steering Committee Member of the IEEE Symposium on Diagnostics for Electrical Machines, Power Electronics and Drives. Finally, he serves as an Associate Editor for the IEEE Transactions on Industry Applications and the IEEE Transactions on Energy Conversion.

Marios Salinas holds a 5-year Diploma (MSc equivalent) in Electrical and Computer Engineering, specialising in induction motor fault diagnosis from the Technical University of Crete, Greece (2024). He is currently a PhD student in the same School working on fault diagnosis and condition monitoring of electrical machines in the industrial and renewable energy sector. He is currently working as a researcher for the EU HORIZON and UKRI-funded project "MEGA PTO WAVE" aiming to develop innovative diagnostic methods for permanent magnet generators used for wave energy harvesting.

Nikolaos Trachalakis is a recent graduate from the School of Electrical and Computer Enginnering, Technical University of Crete, Greece (2024) holding a 5-year Diploma (MSc equivalent) in Electrical and Computer Engineering. His research focused on electromagnetic analysis and fault detection in industrial induction motors.

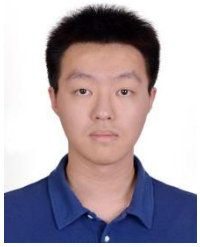

Zihao Song (Student Member, IEEE, '24) received the B.Eng. and the M.Sc. degrees in electronic and electrical engineering from the University of Sheffield, Sheffield, UK, Department of Electronic and Electrical Engineering (EEE), in 2022 and 2023, respectively. Since 2023, he is a doctoral candidate (PhD student) in diagnostics for electrical machines and drives with the Electrical Machines and Drives research group of the School of Electrical and Electronic Engineering, University of Sheffield, Sheffield, U.K. His research interests include condition monitoring of electrical machines, fault detection and diagnostics, finite element modelling for fault analysis, and development of fault detection methods.

Panagiotis A. Panagiotou (M'22) received the 5-year Diploma (B.S. & M.Eng.) from the Department of Electrical and Computer Engineering of the University of Patras, Patras, Greece, in 2015, and the M.Sc. degree in Complex Systems and Network Theory from the Department of Mathematics of the Aristotle University of Thessaloniki, Thessaloniki, Greece, in 2017. He received the Ph.D. degree in fault diagnostics of electrical machines from Coventry University, Coventry, U.K., in 2020. In 2021, he joined the Department of Electronic and Electrical Engineering of the University of Sheffield, Sheffield, U.K., as a postdoctoral research associate at the Rolls-Royce University Technology Centre for Advanced Electrical Machines of the University of Sheffield. Since 2022, he is a Lecturer in electrical machines with the School of Electrical and Electronic Engineering of the University of Sheffield. His research interests include condition monitoring, fault detection and diagnostics in electrical machines, signal processing for diagnostics, and technologies for the inspection and repair of electrical machines.

Dr. Panagiotou is a member of the IEEE, a member of the Institution of Engineering and Technology (IET, U.K.) and a Fellow of the Higher Education Academy (FHEA), U.K.